Title

All-Printed, Stretchable Zn-Ag2O Rechargeable Battery via Hyperelastic Binder for Self-Powering Wearable Electronics

Journal

Advanced Energy Materials, 7(8)

ISSN

1614-6832

Authors

Kumar, Rajan
Shin, Jaewook
Yin, Lu
et al.

Publication Date

2017-04-01

DOI

10.1002/aenm.201602096

Peer reviewed

All-Printed, Stretchable Zn-Ag_2O Rechargeable Battery via, Hyperelastic Binder for Self-Powering Wearable Electronics

Rajan Kumar, Jaewook Shin, Lu Yin, Jung-Min You, Ying Shirley Meng, and Joseph Wang**

While several stretchable batteries utilizing either deterministic or random composite architectures have been described, none have been fabricated using inexpensive printing technologies. In this study, the authors printed a highly stretchable, zinc-silver oxide (Zn-Ag_2O) battery by incorporating polystyrene-*block*-polyisoprene-*block*-polystyrene (SIS) as a hyperelastic binder for custom-made printable inks. The remarkable mechanical properties of the SIS binder lead to an all-printed, stretchable Zn-Ag_2O rechargeable battery with a ≈2.5 mA h cm^{-2} reversible capacity density even after multiple iterations of 100% stretching. This battery offers the highest reversible capacity and discharge current density for intrinsically stretchable batteries reported to date. The electrochemical and mechanical properties are characterized under different strain conditions. The new stress-enduring printable inks pave ways for further developing stretchable electronics for the wide range of wearable applications.

1. Introduction

The advent of flexible/stretchable electronics has cultivated the next generation of sensors,[1–3] photovoltaics,[4] paper-like displays,[5] wearable/implantable electronics,[6,7] e-textiles,[8] optics,[9] and soft robotics.[10] Unlike their brittle and rigid predecessors, soft electronics can intimately integrate with curvilinear surfaces while withstanding the complex deformations common of human organs, textiles, or robotics.[11] Unfortunately, the progress of stretchable systems, specific to their mobility and independence, is currently constrained by bulky and rigid powering sources.[12,13] Batteries hold the most promise owing to their high power and energy densities, rechargeability, and low-cost.[12] Stretchable batteries have been fabricated through many different approaches, deterministic composite[14,15] and random composite[16–19] architecture.

The deterministic approach relies on subtractive methods to render otherwise rigid materials, with bulk properties, into deterministic structures such as "island-bridge"[20,21] or "cable-type"[15] batteries.[22] By engineering elasticity with high-performance, rigid electrodes, these stretchable batteries can withstand high levels of strain without intrinsically stretching them. The random composite approach embeds percolations of highly conductive fillers (>10^7 S m^{-1}, silver nanowires and carbon nanomaterials) into an elastomeric matrix.[23] Unlike deterministic composite, these devices are intrinsically stretchable as fillers maintain electrical contact by sliding along each other during stretching.[22] Intrinsically stretchable batteries have been reported, but none are completely elastic systems.[16–19] The cycle ability, current density, or areal capacity of these batteries are compromised when a rigid component undergoes large physical strain (Table S1, Supporting Information).[17–19,24] Unfortunately, both deterministic and random composite-designed batteries are not economical because they rely on lithographic,[7,20,25] spray/dip coating,[16,26] or "cut-and-paste"[2,19,27] fabrication routes that are extremely expensive and low-throughput.

Today, printed, non-rechargeable batteries is an emerging market supporting many wearable and disposable electronics, and expected to reach a value of $1.2 billion by 2017, CAGR 46% from 2012.[28] Individual components are fabricated using a single, inexpensive printing step through either dispensing, screen, roll-to-roll, or inkjet printing of composite inks.[24,29] Unlike comparable coating technologies, such as spray or dip coating that may have high throughputs, screen printing can actively control the design that can potentially combine both deterministic and random composites. The higher viscosity requirements of screen printing enable high loadings of conductive fillers toward superior elastic performance and higher battery operation. The rheology of the ink is controlled by the composite formulation of electroactive fillers, a binder, and a specific solvent.[24,29] The binder plays the role of holding the ink components together and in dictating the flexible and stretchable nature of the inks. The synthesis of stretchable inks is highly challenging since the battery experiences significantly higher strain levels during stretching as compared to just bending. The printing technologies and random composite-based inks can be used to fabricate cost-effective and intrinsically stretchable batteries.[1,30] The fundamental challenge of using random composite is that the electrochemical properties of the fillers and elastic matrix are mutually detrimental to the other. This approach becomes overwhelmingly challenging for printed, stretchable batteries with poorly conductive, electroactive fillers (≈10^5 S m^{-1}), thus the need for new innovations in highly elastic matrix is imperative.[22] Specially formulated inks must be formulated to allow the printed batteries to be stretched 100% multiple times.

R. Kumar, Dr. J. Shin, L. Yin, Dr. J.-M. You, Prof. Y. S. Meng, Prof. J. Wang
University of California San Diego
NanoEngineering Department
9500 Gilman Dr., La Jolla, CA 92093, USA
E-mail: shmeng@ucsd.edu; josephwang@ucsd.edu

DOI: 10.1002/aenm.201602096

Here in, we report the first all-printed stretchable zinc-silver oxide (Zn-Ag_2O) rechargeable battery using low-cost screen printing of highly elastic, conductive inks. The novelty of this work hinges on the attractive hyperelastic properties (≈1300% elongation) of polystyrene-*block*-polyisoprene-*block*-polystyrene (SIS) as a new elastic binder for stretchable batteries. Due to unique block polymeric structure of long polyisoprene chain and short polystyrene terminal ends, SIS has superior elasticity and simpler processing compared to common elastomers, e.g., exoflex, that require an additional curing (vulcanization) step to form the 3D crosslinked network to impart truly elastic behavior (Table S2, Supporting Information).[1,31–33] Owing to its unrivaled properties, SIS can be incorporated in higher loadings while maintaining the mechanical and electrochemical properties of the battery.[34,35] The resulting rechargeable Zn-Ag_2O battery demonstrates a reversible capacity density of ≈2.5 mA h cm^{-2} even after multiple iterations of 100% stretching. To our knowledge, this represents an intrinsically stretchable battery with the highest reversible capacity and discharge current density, fabricated by inexpensive printed technologies, reported to date. The new SIS-based printed battery can withstand other severe torsional strains relevant to the wearer's movement. The mechanical properties of the stretchable battery are evaluated using digital image correlation (DIC) and scanning electron microscopy (SEM) and its attractive electrochemical cycling, impedance and mechanical properties are presented.

2. Results

The attractive mechanical properties of the SIS binder lead to intrinsically stretchable and rechargeable printable Zn-Ag_2O battery that can withstand a variety of severe mechanical strains. Two stretchable batteries were printed in a "NANO" design directly on top of the thermoplastic polyurethane (PU) head sealed onto the spandex (**Figure 1**A). On the "NANO" current collector, the respective electrodes were printed to form two batteries of an "NA" and an "NO" designed connected in series to power a 3 V wearable-based LED (Figure 1B). An additional seal between "A" and the second "N" was applied to avoid the short circuit. The stretchable "NANO" battery maintains a constant LED brightness regardless of severe torsional strain (Figure 1C), indentations (Figure 1D), 100% uniaxial stretching (Figure 1E), and biaxial stretching (Figure 1F and Videos S1, S2, Supporting Information). The printed battery can thus withstand high tensile stress without incurring any macrolevel cracking or debonding.

A non-contact optical method called DIC has been utilized for strain mapping of the printed carbon electrodes of different SP:SIS ratios (1:1, 1:2, and 1:3) upon their stretching. DIC is frequently employed as a high-resolution imaging tool to analyze the deformations of macroscale objects in real-time to identify faults in materials or design.[36] In this technique, the surface is prepared with a white coat and random black speckle, a grayscale intensity pattern can be mapped for each pixel in

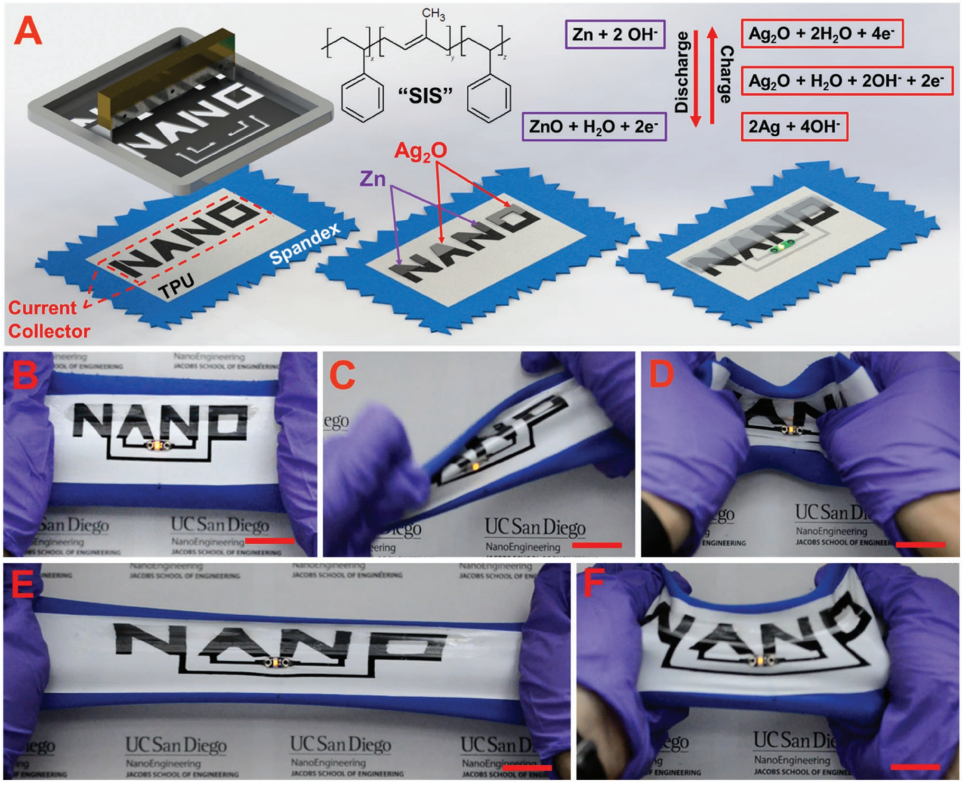

Figure 1. A) Screen-printing steps of a Zn-Ag_2O battery on a stretchable textile using a SIS binder. Inset: Redox charge and discharge reaction. Photographs of sealed battery while being B) 0% stretched, C) twisted, D) indentation strains, E) 100% stretched, and F) biaxial stretched. Scale Bar: 2.25 cm

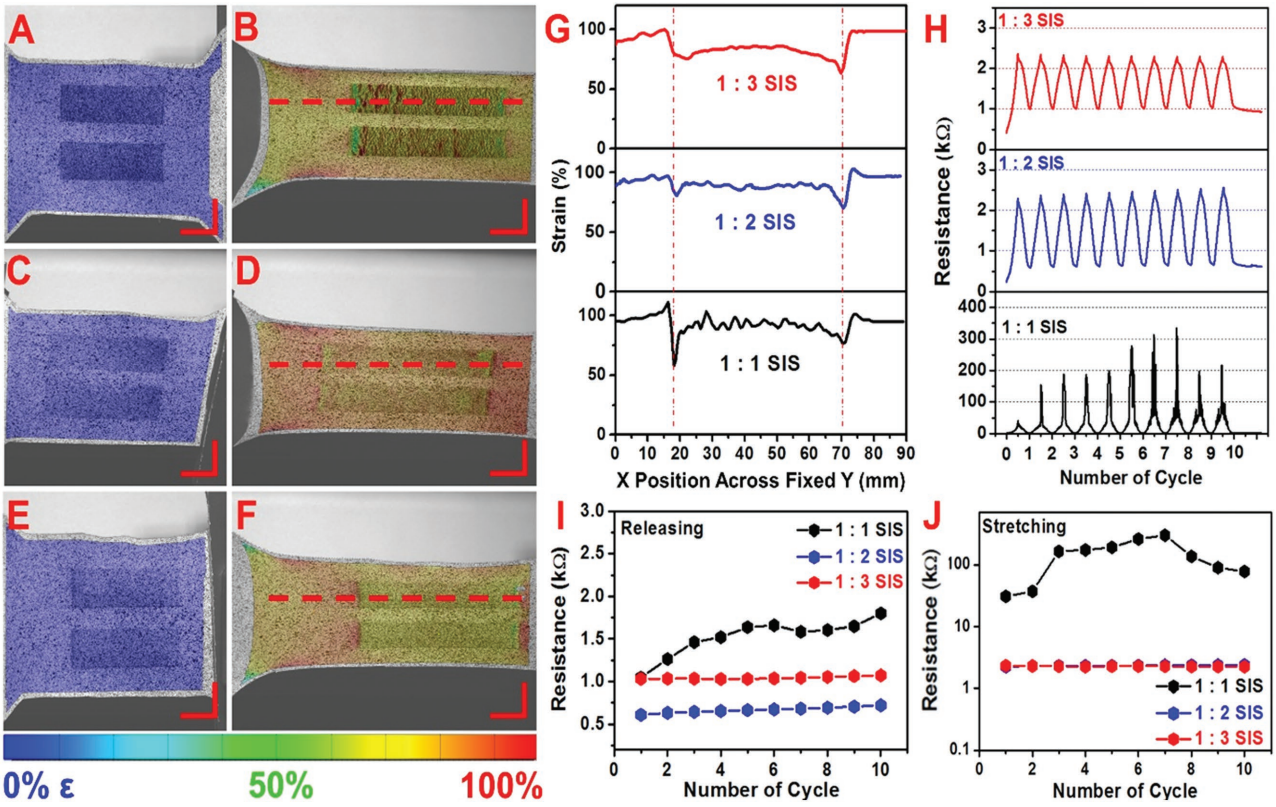

Figure 2. 2D strain mapping of the rectangular carbon electrodes at 0% stretching (A) 1:1 ratio, C) 1:2 ratio, and E) 1:3 ratio) to 100% stretching (B) 1:1 ratio, D) 1:2 ratio, and F) 1:3 ratio). G) The strain plotted over the dotted line. H) Respective resistance monitored during the ten cycles of 100% stretching iterations. Respective resistances at I) release and J) stretching. Scale Bar: 1.0 cm.

the digital image of the sample.[36] The incremental displacements of each speckle on the surface can be tracked using this grayscale intensity between images before and after the deformation.[36] Algorithms are used to patch pixels into groups called facets, where strain on the object's surface can be correlated based on the changing dimensions of the facet.[36] The strain (ε_x,ε_y) is calculated by the amount of change in size of the facet (traced by DIC) divided by the original size of the facet[36] Lower strain value indicates that pixel did not change much in that particular spot. If the pixel does not change much, this indicates that the facet or the location on the sample was hard to deform. Sudden increase in the strain indicates plastic deformations caused by the cracks.

A 2D strain mapping (ε_x) of the rectangular carbon electrodes (1:1 ratio, 1:2 ratio, and 1:3 ratio) is demonstrated from 0% stretching (**Figure 2**A,C,E) to 100% stretching in the *x*-axis (Figure 2B,D,F and Videos S3–S5, Supporting Information). As the electrodes are stretched, there are significant changes in the strain mapping. For all the electrodes, the strain on the textile surface is generally higher than that of the electrode surfaces (Figure 2G). While a significant drop in the strain is observed at the interface between textile and the electrode, the 1:1 ratio electrode shows the larger drop. Furthermore, the strain distribution on the electrode surface is highly irregular for the 1:1 ratio electrode, and is correlated to the physical cracks of the electrode. Such strain distributions are more uniform for the higher SIS-content electrodes, suggesting that electrodes with higher SIS content are not physically cracked in the optical scale.

In addition to the DIC analysis, change in resistance during the stretching cycles have been monitored (Figure 2H). At stretched state, the 1:1 ratio electrode has consistently high and unstable resistance due to the electrode cracking observed from the DIC (Figure 2J). For the other two electrodes, with higher SIS content, the resistance values are stable and similar at the stretched state at around 2.3 kΩ. However, when the electrodes are released from the stretching motion, the 1:2 ratio electrode consistently demonstrates the lowest resistance among the three electrodes with 0.65 kΩ (Figure 2I). In addition to DIC analysis and resistance studies, stress and conductivity of the three composite ratios were simultaneously measured as they were strained. As shown in shown in **Table 1** and Figure S5 in the Supporting Information, these measurements can compare the Young's modulus, conductivity at 0% strain, conductivity

Table 1. Mechanical characterization of SP:SIS composite inks.

Composite SP:SIS ratios	Young's modulus [Psi]	Conductivity at 0% strain [S m^{-1}]	Conductivity prior to break [S m^{-1}]	Elongation at break [%]
1:1	–	60	7	9
1:2	725	44	0.68	474
1:3	145	18	0.21	598

prior to break, and elongation at break. Clearly, the 1:2 ratio electrode offers the optimum condition among the three composites, with the most favorable tradeoff between relatively high conductivity and a low Young's modulus. This ratio has thus been utilized to fabricate the carbon current collector electrode for the stretchable Zn-Ag_2O battery.

Although no cracks are observed in the DIC, the resistance still increases upon stretching. Since the DIC can highlight areas of cracking at the macroscale, SEM is utilized to observe physical deformations on the micrometer scale. Morphology of the optimized carbon electrode, Zn electrode, and Ag_2O electrode are observed before, during, and after stretching (**Figure 3**). While no cracks are observed at pristine state, upon stretching, micro cracks are observed. The cracks on these electrodes lead to increase the resistance and limit the electron conduction pathways. Per size of the cracks, carbon electrodes have the smallest cracks compared to those of the Zn and Ag_2O electrodes. For the Zn and Ag_2O electrodes, electrical contacts may be disturbed by such large cracks. Thus, it is important to keep the carbon electrode on the bottom of the Zn and Ag_2O electrodes to maintain the electrical connection. Although the carbon electrode has cracks as well, they are minute and uniformly distributed, which allow the electrical connections to be well preserved. After releasing the electrodes following ten cycles of 100% stretching, both the carbon and Zn electrodes regained their crack-free morphology while Ag_2O displayed only a minor crack.

The electrochemical performance of the stretchable battery has been tested. The first cycle voltage profiles show high discharge capacity (**Figure 4**A). The pristine battery has 3.78 mA h cm^{-2} and stretching battery has 3.94 mA h cm^{-2} capacity. Upon stretching, the discharge capacity has slightly increased which is attributable to the enlarged active surface area from the cracks formed during stretching. It is notable that the average voltage decreases after stretching. This decreased voltage is due to the increased polarization and is more detrimental during the charge. The stretching battery has higher discharge capacity whereas the charge capacity is significantly lower than the pristine. Due to the increased polarization, the second oxidation reaction, $Ag_2O + 2OH^- + 2e^- \rightarrow 2AgO + H_2O$, from the cathode has not occurred,[17] resulting in lower capacity than the pristine battery during the prolonged cycle (Figure 4B). However, for both cases of batteries, the prolonged cycle discharge capacities are stable up to 30 cycles. The first cycle discharge capacity during the prolonged cycle, the pristine has higher capacity close to 3 mA h cm^{-2} compared to that of the stretching battery of about 2.5 mA h cm^{-2}.

An electrochemical impedance spectroscopy (EIS) has been carried out to examine the polarization during the mechanical perturbation. The electrochemical cycling performance of the stretching battery is examined after ten times of 100% stretching. EIS for the pristine and stretched battery are obtained at pristine state and when the battery is 100% stretched in order to understand the difference in polarization of the battery (Figure 4C,D). In the EIS, high, medium, and low frequency regions are identified with the light and dark green dotted lines. All three regions have charge transfer resistance and the constant phase elements. The depressed semicircle in the medium frequency region represents the charge transfer resistance of the ions in the electrolyte or the charge of the Zn

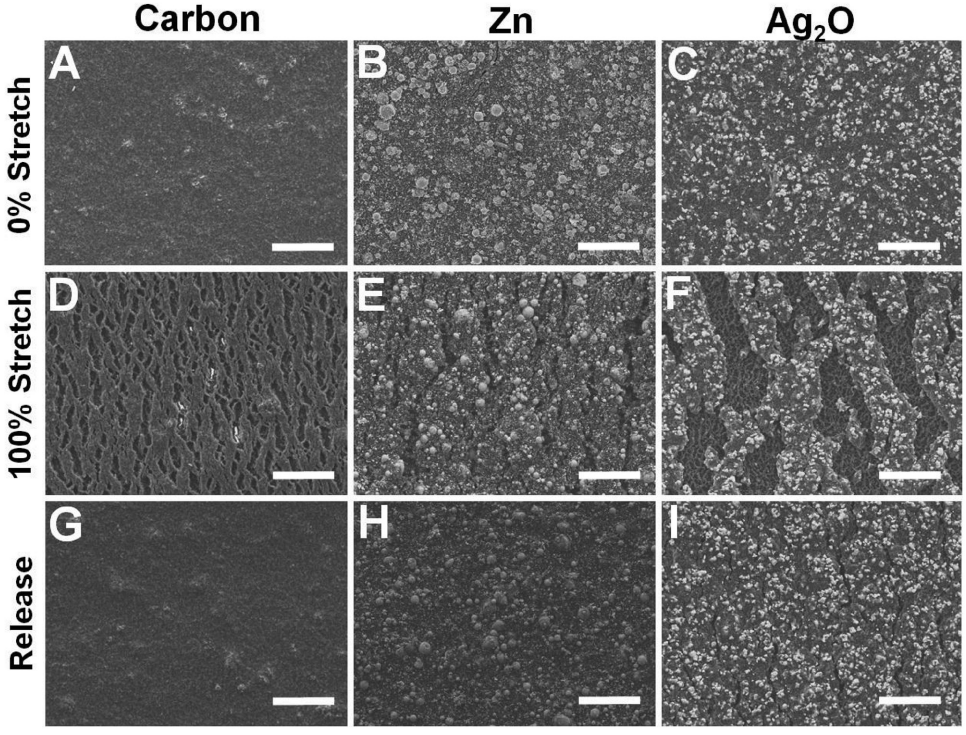

Figure 3. A) SEM images of the carbon current collector, B) Zn electrode, and C) Ag_2O electrode as printed, D) carbon current collector, E) Zn electrode, and F) Ag_2O electrode 100% stretched, and G) carbon current collector, H) Zn electrode, and I) Ag_2O electrode released after ten 100% stretching iterations. Scale bar: 50 μm.

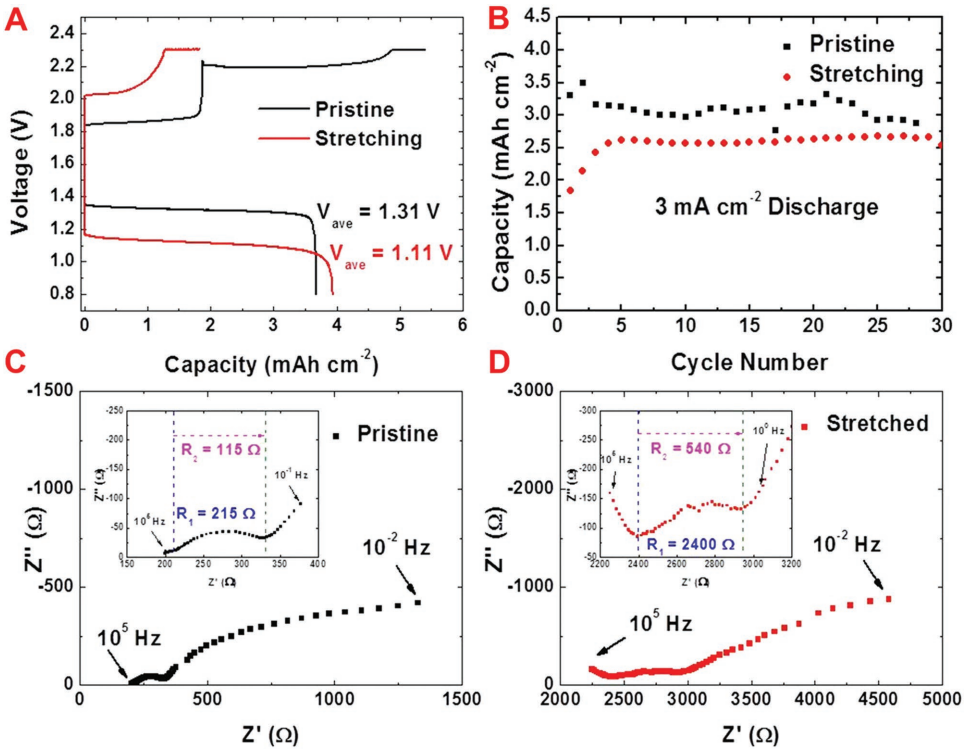

Figure 4. A) The first cycle voltage profile of the stretchable battery cycled with 2 mA h cm^{-2}. B) The discharge capacity during prolonged cycle, cycled with 3 mA h cm^{-2}. Stretching battery has been 100% stretched ten times before the electrochemical cycling. C) EIS of the pristine battery. D) EIS of the battery stretched to 100%.

anode and Ag_2O cathode.[37] The diameter of the depressed semicircle can be used to estimate the charge transfer resistance (R_2) on the electrodes. After being stretched, the R_2 increases from 115 to 540 Ω. Before the depressed semicircle, the charge transfer resistance is representative of the uncompensated resistance or the carbon current collector electrode in the high frequency region.[37] The light green dotted line is used to estimate the charge transfer resistance (R_1) of the current collector. After being stretched, the R_1 increases from 215 to 2400 Ω. After the depressed semicircle, the charge transfer resistance is related to the electrochemical reaction in the low frequency region. This highly resistive behavior is commonly observed in the EIS when the spectrum is obtained at the voltage in which electrochemical reaction can occur.[38]

3. Discussion

The above results have illustrated the attractive properties of the SIS elastomer as the binder for highly stretchable low-cost screen-printed batteries. As a triblock copolymer (ABA), SIS forms a phase separation of soft isoprene blocks that are physically crosslinked by nanoclusters glassy styrene blocks.[35,39,40] This self-assembled elastic network gives SIS superior elastic properties and the lack of a vulcanization step simplifies ink synthesis.[39,40] The vulcanization is a well-known process that crosslinks the polymers where entropy drives these materials to forcibly retract to their original shape after an applied deformation is removed.[31,39,40] In addition, the SIS demonstrated excellent adhesion to the substrate, obviating the need for adding non-conductive surfactants commonly used to prevent delamination.[1,30,33] The strong adhesion of the ink can be attributed to the high tack quality of polyisoprene group of the SIS binder.[34,40] Such ability for imparting stretchability has led to printable batteries that display high performance following multiple severe mechanical strains.

DIC has been shown useful to map the tensile strain for various stretchable electronic device composed of different materials and unique compositions. In Figure 2A–F, the strain mapping is different between printed traces based on three SP:SIS ratios because of these printed electrodes display a different mechanical behavior that is dependent upon the ratios of inelastic or elastic during the ink synthesis. The interfaces between the materials of different elasticities such as printed electrode and the PU substrate can also be mapped. At the interface, an abrupt decrease in the strain is observed for all electrodes. This is because at the interfaces, the electrode is thickest. When squeeze moves the ink across the cavities of the stencil, most amount of ink is accumulated at the edges. Upon curing, the electrode is thickest at the edges. Because the edges are thicker than the core or outside of the edges, it is harder to displace these regions. In order to compensate for the low strain on the interfaces, the textiles, and thin prints exhibit the higher strains.

The stress and conductivity versus strain measurements provided an additional material characterization of the SP:SIS composites. As shown in Table 1, the 1:1 ratio composite—as an individual unbound film—has poor mechanical resilience

but the highest initial conductivity. In comparison, resistance measurements on the 1:1 ratio composite printed on the stretchable Exoskin substrate demonstrated improved durability, reflecting its behavior as a stiff-island on a soft matrix. The 1:2 ratio composite exhibits a trade-off of durability and conductivity between the two extreme composite ratios (1:1 to 1:3). Such optimal composite behavior is attributed to the engineering of rigid, conductive fillers with an elastic polymer binder toward developing highly stretchable inks for specific application. The voltage profiles of the first cycle show that the voltage plateau decreases after stretching (Figure 4A). The lower voltage plateau indicates that the polarization increased. However, the SEM images reveal that the cracks formed during stretching disappear upon the release (Figure 3). This discrepancy is likely due to the presence of the electrolyte. Although the physical cracks may disappear, the electrolyte may soak in between the cracks and hinder the electrical pathway. Furthermore, the stretched electrode shows the highest areal capacity during the first cycle (Figure 4A). This is because the electrolyte has soaked the cracks and has significantly increased the active surface area. When the electrode is stretched, new surface area is exposed and the electrolyte soaks the new surface. The stretched electrodes have the wider active surface area.

In the EIS results, both R_1 and R_2 increase upon stretching (Figure 4C,D). The degree of rise is significantly different from each other. The R_1 escalates by a factor of 11.2 whereas the R_2 grows by a factor of 4.70. The R_1 is contributed by stretching the carbon current collector electrode and R_2 is mostly contributed by the anode and cathode. While both the resistance values increase with respect to the stretching, the R_1 increases more significantly. This suggests that the deformations derive the impedance in electric connections more so than the electrodes. If the mechanical strain on the current collector layer can be alleviated, the electrochemical performance can be greatly enhanced. One of the buckling device configurations, a serpentine configuration or cable type of configuration can be employed to alleviate the mechanical strain.[1] Since these configurations have been widely known to reduce the mechanical strain,[1] the electrochemical performance can be largely improved with intrinsically stretchable electrodes.

4. Conclusions

In summary, we have demonstrated a successful fabrication and operation of a printable, highly stretchable rechargeable Zn-Ag_2O battery based on a hyperelastic SIS as a binder. All the components of the battery are printed using high-throughput and inexpensive screen printing. In order to obtain the maximum performance of stretchable electronics, systematic and vigorous mechanical studies utilizing DIC and SEM have been conducted. The rechargeable Zn-Ag battery has reversible capacity density of ≈2.5 mA h cm^{-2} at 3 mA cm^{-2} discharge current density even after the repeated cycles of 100% stretching iterations. Such performance represents an intrinsically stretchable battery with the highest reversible capacity and discharge current density. The excellent resiliency against severe battery stretching is attributed to the superior elasticity of the SIS binder associated with its long polyisoprene chains with well-spaced, physically cross-linking styrene domains.[41] The first DIC was implemented for localized strain analysis of stretchable electronics. Further optimization of the printed deterministic structures, new materials, and expansion of DIC in the printing design (like the implementation of deterministic structures or sandwich battery designs), have the potential to enhance the electrochemical performance and the understanding of the mechanical properties of SIS-based batteries. More importantly, SIS has the potential to outperform previous printed, stretchable electronics and is expected to pave the way to enhance other forms of energy storage technologies, including Li-ion batteries, supercapacitors, and photovoltaics toward self-power stretchable electronics. These SIS-based printed devices would allow several degrees of freedom relevant to the wearer's movement, and can be conformably utilized in diverse real-life situations.

5. Experimental Section

Chemicals and Reagents: Super-P Conductive Carbon Black (SP), toluene (Alfa Aesar), 200 proof Koptec (Decon Labs, King of Prussia, PA), Zn powder (Alfa Aesar), Ag_2O powder (Alfa Aesar), Bi_2O_3 (Alfa Aesar). Universal mold release (Smooth-On). KOH, LiOH, polyacrylic acid, and SIS (14% styrene) were purchased from Sigma Aldrich.

Elastic Composite Inks Preparation: The elastic carbon current collector ink was prepared by first dissolving 1.10 g of SIS pellets in 5 mL of toluene with an analog vortex mixer (VWR) for 1 h. Toluene was chosen as the SIS solvent due to its similar Hillenbrand solubility parameters.[42] Then 0.6 g of SP was mixed into the SIS solution in a dual asymmetric centrifugal mixer (Flacktek Speedmixer, DAC 150.1 KV-K) at 3000 rpm for 5 min. After cooling the ink, 4 g of yttria stabilized zirconia grinding beads (3 mm diameter, Inframat Advanced Materials) and additional 4 mL of toluene were added and underwent further mixing of 3000 rpm for 30 min to thoroughly mix and achieve optimum viscosity.[43] The elastic Zn ink was prepared by first dissolving 0.6 g of SIS pellets in 2.8 mL of 80% (v/v) toluene and 20% (v/v) ethanol with analog vortex mixer for 1 h. Then, 3.4 g of composite Zn powder (30 wt% SP, 60 wt% Zn, and 10 wt% Bi_2O_3)[44] were mixed into the SIS solution in the dual asymmetric centrifugal mixer at 3000 rpm for 5 min. After cooling the ink in air, 2 g of the yttria-stabilized zirconia grinding beads and additional 1.5 mL of the toluene/ethanol solution were added and underwent further mixing of 3000 rpm for 30 min. The elastic Ag_2O ink was prepared by first dissolving 0.6 g of SIS pellets in 2.8 mL of 80% (v/v) toluene and 20% (v/v) ethanol with analog vortex mixer for 1 h. Then, 3.0 g of composite Ag_2O powder (20 wt% SP and 80 wt% Ag_2O)[44] were mixed into the SIS solution in the dual asymmetric centrifugal mixer at 3000 rpm for 5 min. After cooling the ink in air, 2 g of the yttria-stabilized zirconia grinding beads and additional 1.5 mL of the toluene/ethanol solution was added and underwent further mixing of 3000 rpm for 30 min.

Stretchable Zn-Ag_2O Battery Fabrication: The printing process employed an MPM-SPM semi-automatic screen printer (Speedline Technologies, Franklin, MA). The bold "NANO" and rectangle patterns were designed in AutoCAD (Autodesk, San Rafael, CA) and patterned into a stainless steel through-hole 12 in. by 12 in. framed stencils with a thickness of 100 m (Metal Etch Services, San Macros, CA). A thermoplastic PU sheet (ST604, Bemis Worldwide, Shirley, MA) was thermally bonded to smoothen the surface royal-blue colored high performance spandex (Spandex World, New York, NY) using a typical drying iron (T-fal Ultraglide, Parsippany, NJ). A Keyence VHX1000 optical profiler measured the surface roughness between the ink printed directly on textile and TPU bonded textile (Figure S1A,B, Supporting Information). First, carbon ink was used to print the entire "NANO" design as the current collector onto the Bemis bonded textile and cured

in an oven at 80 °C for 15 min. Subsequently, an anode electrode was printed with the Zn ink on the top half of both letter "N" carbon prints and cured in an oven at 80 °C for 15 min. Lastly, a cathode electrode was printed with the Ag_2O ink on the top half of the letters "A" and "O" carbon prints and cured in an oven at 80 °C for 15 min. This design produces two batteries that are connected in series. The outline of the battery was heat-sealed with 26 µm thick PU sheet (Delstar Technologies Inc. Middletown, DE). The sealed battery was filled with the electrolyte formulated from the previous epidermal battery.[44] The "NANO" battery design was connected to a textile-embedded 3 V yellow LED (Lilypad, Sparkfun, Niwot, CO). A complete detailed schematic of the device fabrication is demonstrated in Figure S2 in the Supporting Information. The DIC, SEM, and electrochemical tests were conducted using a pair of 0.9 cm by 3 cm rectangle for the current collector layer and 0.7 cm by 0.9 cm rectangle for the cathode and anode electrodes on a pre-applied PU film commercially named as 9EX-2497P Exoskin (Dartex Coatings Inc., Slatersville, RI).

DIC Tensile Stress Analysis: Carbon current collectors based on three different SP:SIS ratios (1:1, 1:2, and 1:3) were printed on a dog bone shaped cutouts of Exoskin. The carbon inks were using the same SIS solution as the earlier carbon ink. A while spray paint (Flat White Prime, Rust-oluem, Vernon Hills, IL) then a random speckle black pattern (Flat Black Prime, Rust-oluem, Vernon Hills, IL) were lightly sprayed on the printed samples. The printed samples were stretched using a motorized test stand (Mark-10, Copiague, NY) at a constant speed while a pair of high resolution, digital charge coupled device cameras was recording a video of the sample from the relaxed to stretched state of 100%. A commercial software GOM ARAMIS (Trillion Quality Systems, Plymouth Meeting, PA) was used to convert the video into single frames for strain mapping. The black speckle on the white coating can create a grayscale matrix per pixel, which tracks the surface displacements of the deformed materials.[45] Mathematical correlation functions were applied to grayscale distribution from the speckle patterns and were analyzed among images before and after the deformation.[36,45]

Mechanical and Conductivity Characterization of SIS Composite Inks: The three current collector electrodes from the DIC experiment were used to measure the resistance during and after the stretching cycles. The sample preparation was same as the DIC experiment. The stretching tests were conducted on a custom stretching stage (Figure S3A,B, Supporting Information) of a motorized linear stage and controller (A-LST0250A-E01 Stepper Motor and Controller, Zaber Technologies, Vancouver, Canada). The samples were programmed to constantly stretch at a speed of 0.1 cm s^{-1} from 0% to 100% and back to 0% as one cycle. The resistance was measured at 22 pt s^{-1} using a digital multimeter (Agilent, Santa Clara, CA) during the ten cycles. The speed and length of the physical strain were programmed into a scripting software (Zaber console, Zaber Technologies, Vancouver, Canada). Additional mechanical characterization of the composites such as Young's modulus, elongation at break, conductivity at 0% strain, and conductivity prior to break were conducted. The same composite SP:SIS ratios (1:1, 1:2, and 1:3) were prepared by printing on glass slides pre-coated with universal mold release. After curing the samples, the printed samples were easily released from the glass slide and mounted to the custom stretching stage. On one end of the stage, the mount was connected to a digital force gauge (Mark-10, Copiaque, NY) to measure the force applied while the sample was being strained continuously by motorized linear stage. The resistance was measured simultaneously using a digital millimeter. Further calculations based on resistance and force measurements were completed to compare the stress (kN m^{-2}) and conductivity (S m^{-1}) of the composite inks as they are strained.

SEM of Stretched Electrodes: The printed carbon electrode, Zn electrode, and Ag_2O electrode were adhered onto a SEM holder. The pristine samples were adhered as printed without any stretching. The stretched samples were adhered with a 100% stretch. The relaxed samples were adhered after the electrodes were repeatedly stretched 100% for ten cycles. The images were taken using 10 kV energy source using FEI/Philips XL30 ESEM (Philips).

Electrochemical Properties: All electrochemical tests were conducted at room temperature. The electrochemical cycling tests were conducting with Arbin electrochemical cycler channels. Electrochemical cycling tests were conducted with 2 mA cm^{-2} first formation cycle and 3 mA cm^{-2} discharge current, and 2 mA cm^{-2} charge current for the subsequent cycles. The discharge cut-off voltage was 0.8 V and the charge cut-off voltage was 2.3 V with 20 min constant voltage step. For bending and stretching electrodes, the batteries were electrochemically cycled after being relaxed for 30 min. The EIS was conducted using a 10^5–10^{-2} Hz frequency range with 10 mV amplitude using Solartron 1287 electrochemical interface. All EIS tests were conducted at the open circuit voltage upon the formation cycle.

Supporting Information

Supporting Information is available from the Wiley Online Library or from the author.

Acknowledgements

R.K. and J.S. contributed equally to this work. This publication was supported by Advanced Research Projects Agency-Energy (DE-AR0000535). R.K. acknowledges the National Science Foundation Graduate Research Fellowship under Grant No. (DGE-1144086). Any opinion, findings, and conclusions or recommendations expressed in this material are those of the authors(s) and do not necessarily reflect the views of the Department of Energy and National Science Foundation. The authors would like to thank Johnathan Pickworth and his team at Trilion Quality Systems (Plymouth Meeting, PA) for providing GOM ARAMIS for the DIC analysis of the stretchable battery, Bemis Worldwide for samples of their ST604 TPU, and Dartex Coatings for their Exoskin textile. This work was performed in part at the San Diego Nanotechnology Infrastructure (SDNI), a member of the National Nanotechnology Coordinated Infrastructure, which is supported by the National Science Foundation (Grant ECCS-1542148). Lastly, the authors thank P. Y. Meng and Lin Xia for assistance in the sample preparation.

Received: September 20, 2016
Revised: October 27, 2016
Published online:

[1] A. J. Bandodkar, I. Jeerapan, J.-M. You, R. Nuñez-Flores, J. Wang, *Nano Lett.* **2016**, *16*, 721.
[2] H. Lee, T. K. Choi, Y. B. Lee, H. R. Cho, R. Ghaffari, L. Wang, H. J. Choi, T. D. Chung, N. Lu, T. Hyeon, S. H. Choi, D.-H. Kim, *Nat. Nano* **2016**, *11*, 566.
[3] a) R. Cánovas, M. Parrilla, P. Mercier, F. J. Andrade, J. Wang, *Adv. Mater. Technol.* **2016**, *1*, 1600061; b) M. Amjadi, K.-U. Kyung, I. Park, M. Sitti, *Adv. Funct. Mater.* **2016**, *26*, 1678; c) A. J. Bandodkar, I. Jeerapan, J. Wang, *ACS Sens.* **2016**, *1*, 464.
[4] a) J. Lee, J. Wu, M. Shi, J. Yoon, S.-I. Park, M. Li, Z. Liu, Y. Huang, J. A. Rogers, *Adv. Mater.* **2011**, *23*, 986; b) D. J. Lipomi, B. C. K. Tee, M. Vosgueritchian, Z. Bao, *Adv. Mater.* **2011**, *23*, 1771.
[5] a) T. Yokota, P. Zalar, M. Kaltenbrunner, H. Jinno, N. Matsuhisa, H. Kitanosako, Y. Tachibana, W. Yukita, M. Koizumi, T. Someya, *Sci. Adv.* **2016**, *2*, e1501856; b) J. Liang, L. Li, X. Niu, Z. Yu, Q. Pei, *Nat. Photonics* **2013**, *7*, 817.
[6] a) S. Imani, A. J. Bandodkar, A. M. V. Mohan, R. Kumar, S. Yu, J. Wang, P. P. Mercier, *Nat. Commun.* **2016**, *7*, 11650; b) J. Kim, I. Jeerapan, S. Imani, T. N. Cho, A. Bandodkar, S. Cinti, P. P. Mercier, J. Wang, *ACS Sens.* **2016**, *1*, 1011; c) A. J. Bandodkar, W. Jia, C. Yardımcı, X. Wang, J. Ramirez, J. Wang, *Anal. Chem.* **2015**, *87*,

394; d) P. Kassal, J. Kim, R. Kumar, W. R. de Araujo, I. M. Steinberg, M. D. Steinberg, J. Wang, *Electrochem. Commun.* **2015**, *56*, 6; e) X. Huang, Y. Liu, H. Cheng, W.-J. Shin, J. A. Fan, Z. Liu, C.-J. Lu, G.-W. Kong, K. Chen, D. Patnaik, S.-H. Lee, S. Hage-Ali, Y. Huang, J. A. Rogers, *Adv. Funct. Mater.* **2014**, *24*, 3846; f) D. Son, J. Lee, S. Qiao, R. Ghaffari, J. Kim, J. E. Lee, C. Song, S. J. Kim, D. J. Lee, S. W. Jun, S. Yang, M. Park, J. Shin, K. Do, M. Lee, K. Kang, C. S. Hwang, N. Lu, T. Hyeon, D.-H. Kim, *Nat. Nano* **2014**, *9*, 397.

[7] L. Xu, S. R. Gutbrod, Y. Ma, A. Petrossians, Y. Liu, R. C. Webb, J. A. Fan, Z. Yang, R. Xu, J. J. Whalen, J. D. Weiland, Y. Huang, I. R. Efimov, J. A. Rogers, *Adv. Mater.* **2015**, *27*, 1731.

[8] a) C. Wu, T. W. Kim, F. Li, T. Guo, *ACS Nano* **2016**, *10*, 6449; b) Y. Meng, Y. Zhao, C. Hu, H. Cheng, Y. Hu, Z. Zhang, G. Shi, L. Qu, *Adv. Mater.* **2013**, *25*, 2326.

[9] S. I. Park, D. S. Brenner, G. Shin, C. D. Morgan, B. A. Copits, H. U. Chung, M. Y. Pullen, K. N. Noh, S. Davidson, S. J. Oh, J. Yoon, K.-I. Jang, V. K. Samineni, M. Norman, J. G. Grajales-Reyes, S. K. Vogt, S. S. Sundaram, K. M. Wilson, J. S. Ha, R. Xu, T. Pan, T.-i. Kim, Y. Huang, M. C. Montana, J. P. Golden, M. R. Bruchas, R. W. Gereau Iv, J. A. Rogers, *Nat. Biotechnol.* **2015**, *33*, 1280.

[10] N. Lu, D.-H. Kim, *Soft Rob.* **2013**, *1*, 53.

[11] a) D. J. Lipomi, *Adv. Mater.* **2016**, *28*, 4180; b) D.-H. Kim, J. A. Rogers, *Adv. Mater.* **2008**, *20*, 4887.

[12] S. Berchmans, A. J. Bandodkar, W. Jia, J. Ramirez, Y. S. Meng, J. Wang, *J. Mater. Chem. A* **2014**, *2*, 15788.

[13] a) R. E. Sousa, C. M. Costa, S. Lanceros-Méndez, *ChemSusChem* **2015**, *8*, 3539; b) *Stretchable Electronics* (Ed: T. Someya), Wiley-VCH Verlag GmbH & Co. KGaA **2012**, p. 287.

[14] a) Z. M. Song, X. Wang, C. Lv, Y. H. An, M. B. Liang, T. Ma, D. He, Y. J. Zheng, S. Q. Huang, H. Y. Yu, H. Q. Jiang, *Sci. Rep.* **2015**, *5*, 10988; b) S. Jung, S. Hong, J. Kim, S. Lee, T. Hyeon, M. Lee, D. H. Kim, *Sci. Rep.* **2015**, *5*, 17081; c) S. Xu, Y. H. Zhang, J. Cho, J. Lee, X. Huang, L. Jia, J. A. Fan, Y. W. Su, J. Su, H. G. Zhang, H. Y. Cheng, B. W. Lu, C. J. Yu, C. Chuang, T. I. Kim, T. Song, K. Shigeta, S. Kang, C. Dagdeviren, I. Petrov, P. V. Braun, Y. G. Huang, U. Paik, J. A. Rogers, *Nat. Commun.* **2013**, *4*, 4479.

[15] a) Y. H. Kwon, S. W. Woo, H. R. Jung, H. K. Yu, K. Kim, B. H. Oh, S. Ahn, S. Y. Lee, S. W. Song, J. Cho, H. C. Shin, J. Y. Kim, *Adv. Mater.* **2012**, *24*, 5192; b) A. M. Zamarayeva, A. M. Gaikwad, I. Deckman, M. Wang, B. Khau, D. A. Steingart, A. C. Arias, *Adv. Electron. Mater.* **2016**, *2*, 1500296.

[16] A. M. Gaikwad, A. M. Zamarayeva, J. Rousseau, H. W. Chu, I. Derin, D. A. Steingart, *Adv. Mater.* **2012**, *24*, 5071.

[17] S. Berchmans, A. J. Bandodkar, W. Z. Jia, J. Ramirez, Y. S. Meng, J. Wang, *J. Mater. Chem. A* **2014**, *2*, 15788.

[18] C. Y. Yan, X. Wang, M. Q. Cui, J. X. Wang, W. B. Kang, C. Y. Foo, P. S. Lee, *Adv. Energy Mater.* **2014**, *4*, 1301396.

[19] G. Kettlgruber, M. Kaltenbrunner, C. M. Siket, R. Moser, I. M. Graz, R. Schwodiauer, S. Bauer, *J. Mater. Chem. A* **2013**, *1*, 5505.

[20] S. Xu, Y. Zhang, J. Cho, J. Lee, X. Huang, L. Jia, J. A. Fan, Y. Su, J. Su, H. Zhang, H. Cheng, B. Lu, C. Yu, C. Chuang, T.-i. Kim, T. Song, K. Shigeta, S. Kang, C. Dagdeviren, I. Petrov, P. V. Braun, Y. Huang, U. Paik, J. A. Rogers, *Nat. Commun.* **2013**, *4*, 1543.

[21] Z. Song, X. Wang, C. Lv, Y. An, M. Liang, T. Ma, D. He, Y.-J. Zheng, S.-Q. Huang, H. Yu, H. Jiang, *Sci. Rep.* **2015**, *5*, 10988.

[22] T. F. O'Connor, S. Savagatrup, D. J. Lipomi, in *Stretchable Bioelectronics for Medical Devices and Systems*, (Eds: A. J. Rogers, R. Ghaffari, D.-H. Kim), Springer International Publishing, Cham, Switzerland **2016**, p. 69.

[23] a) M. D. Dickey, in *Stretchable Bioelectronics for Medical Devices and Systems*, (Eds: A. J. Rogers, R. Ghaffari, D.-H. Kim), Springer International Publishing, Cham, Switzerland **2016**, p. 3; b) M. Park, J. Park, U. Jeong, *Nano Today* **2014**, *9*, 244.

[24] A. M. Gaikwad, G. L. Whiting, D. A. Steingart, A. C. Arias, *Adv. Mater.* **2011**, *23*, 3251.

[25] a) J. A. Fan, W.-H. Yeo, Y. Su, Y. Hattori, W. Lee, S.-Y. Jung, Y. Zhang, Z. Liu, H. Cheng, L. Falgout, M. Bajema, T. Coleman, D. Gregoire, R. J. Larsen, Y. Huang, J. A. Rogers, *Nat. Commun.* **2014**, *5*, 3266; b) C. Yan, X. Wang, M. Cui, J. Wang, W. Kang, C. Y. Foo, P. S. Lee, *Adv. Energy Mater.* **2014**, *4*, 1301396.

[26] H. Kim, J. Yoon, G. Lee, S.-h. Paik, G. Choi, D. Kim, B.-M. Kim, G. Zi, J. S. Ha, *ACS Appl. Mater. Interfaces* **2016**, *8*, 16016.

[27] S. Yang, Y.-C. Chen, L. Nicolini, P. Pasupathy, J. Sacks, B. Su, R. Yang, D. Sanchez, Y.-F. Chang, P. Wang, D. Schnyer, D. Neikirk, N. Lu, *Adv. Mater.* **2015**, *27*, 6423.

[28] Markets and Markets, **2012**.

[29] K. Braam, V. Subramanian, *Adv. Mater.* **2015**, *27*, 689.

[30] J. Kim, R. Kumar, A. Bandokar, J. Wang, *Adv. Electron. Mater.* **2016**, DOI: 10.1002/aelm.201600260.

[31] A. Y. Coran, in *The Science and Technology of Rubber*, 4th ed., Academic Press, Boston **2013**, p. 337.

[32] N. Matsuhisa, M. Kaltenbrunner, T. Yokota, H. Jinno, K. Kuribara, T. Sekitani, T. Someya, *Nat. Commun.* **2015**, *6*, 7461.

[33] A. J. Bandodkar, R. Nuñez-Flores, W. Jia, J. Wang, *Adv. Mater.* **2015**, *27*, 3060.

[34] M. Hu, X. Cai, Q. Guo, B. Bian, T. Zhang, J. Yang, *ACS Nano* **2016**, *10*, 396.

[35] H. Stoyanov, M. Kollosche, S. Risse, R. Waché, G. Kofod, *Adv. Mater.* **2013**, *25*, 578.

[36] P. Bing, Q. Kemao, X. Huimin, A. Anand, *Meas. Sci. Technol.* **2009**, *20*, 062001.

[37] Q. C. Zhuang, S. D. Xu, X. Y. Qiu, Y. L. Cui, L. A. Fang, S. G. Sun, *Prog. Chem.* **2010**, *22*, 1044.

[38] Y. L. Shi, M. F. Shen, S. D. Xu, X. Y. Qiu, L. Jiang, Y. H. Qiang, Q. C. Zhuang, S. G. Sun, *Int. J. Electrochem. Sci.* **2011**, *6*, 3399.

[39] A. Parthiban, *Synthesis and Applications of Copolymers*, John Wiley & Sons, Hoboken **2014**.

[40] B. P. Grady, S. L. Cooper, C. G. Robertson, in *The Science and Technology of Rubber*, 4th ed., Academic Press, Boston **2013**, p. 591.

[41] M. Morton, *Rubber Technology*, Springer Science & Business Media, Dordrecht **2013**.

[42] a) G. L. Robertson, *Food Packaging: Principles and Practice*, CRC Press, Boca Raton **2016**; b) O. Olabisi, L. M. Robeson, M. T. Shaw, *Polymer—Polymer Miscibility*, Academic Press, New York **1979**, p. 195.

[43] a) D. Liu, L.-C. Chen, T.-J. Liu, T. Fan, E.-Y. Tsou, C. Tiu, *Adv. Chem. Eng. Sci.* **2014**, *4*, 14; b) K. Suganuma, *Introduction to Printed Electronics*, Springer, New York **2014**, p. 23.

[44] J.-M. Y. Jaewook Shin, J. Z Lee, R. Kumar, L. Yin, J. Wang, Y. S. Meng, *Phys. Chem. Chem. Phys.* **2016**, *18*, 26376.

[45] S. Hong, D. Sycks, H. F. Chan, S. Lin, G. P. Lopez, F. Guilak, K. W. Leong, X. Zhao, *Adv. Mater.* **2015**, *27*, 4035.